

Enhancing Event-Based Optical Camera Communication Via Dynamic Timing Correction

Matthew Howard
Electrical and Computer Engineering
University of Dayton
Dayton, OH, USA
howardm18@udayton.edu

Keigo Hirakawa
Electrical and Computer Engineering
University of Dayton
Dayton, OH, USA
khirakawa1@udayton.edu

Abstract

Event-based optical sensors have broken the conventional fixed sample rate paradigm of high-speed imaging that normally imposes a harsh limit on sample rate and number of pixels, effectively offering megapixel sensors capable of measuring at 10s of kHz. This behavior is well suited for optical camera communications as has been proposed recently. We use principles of the hardware operation to design an EB-OCC method that improves upon prior works by 25x and facilitates more computationally efficient methods of beacon extraction and tracking. Results presented utilize well calibrated signals in a laboratory environment to aid prediction of performance in the real world. The proposed method achieves up to 75 kbps channel capacity and can compensate for scene motion up to at least the 60 deg/second we reliably generate in the lab.

1. Introduction

As the world becomes more interconnected via wireless communications channels, the available bandwidth in the traditional and regulated radio frequency (RF) bands is steadily becoming a limitation. Wireless optical communication has been proposed to combat this issue, ranging from high bandwidth free-space optical (FSO) channels utilizing lasers [4] to low bandwidth optical camera communications (OCC) channels utilizing cellphone cameras [7]. These optical channels have significant advantages over RF when considering the availability of spectrum as well as the ease of spatial division multiplexing in optical systems.

Recently, methods of event-based OCC (EB-OCC) have been proposed to take advantage of event-based sensors (EBS) that enjoy effectively high temporal sampling without incurring the significant data overhead normally associated with high-speed imaging[8–10]. The techniques in [9, 10] employed on-off keying (OOK) using a modulated

LED without spatial multiplexing to demonstrate channel capacities up to 3 kbps. The method in [8] used a spatially multiplexed marker to achieve up to 118 kbps. Our work utilizes an LED without spatial multiplexing to achieve up to 75 kbps, a 25-fold improvement over prior works.

The channel capacity in EB-OCC such as [10] and [9] appears to be limited by synchronization signal loss and signal-dependent delay, which is illustrated in Figure 1. Here, the EBS observes a “binary chirp” signal (a pulse train with decreasing temporal widths). We superimposed a histogram of observed events over repeated recordings of this binary chirp (events with negative polarity were given “negative” histogram), where the timing of the inceptive events were adjusted so that the first cluster coincides with the first chirp edge (to best illustrate the point). In this plot, one can see that the timing of the events drifts to the right with the decreasing pulse width, implying that synchronization is especially challenging at high transmission rate. The underlying cause of this signal-dependent delay is the analog pixel readout circuit design that introduces frequency and contrast-dependent latency that is difficult to predict. Previous methods have addressed this by shortening the packet sizes, resulting in increased overhead associated with frequently inserting the synchronization markers.

Instead, our proposed method seeks to extract *trends* for signal delay over time, which is subsequently used for synchronization to compensate for the timing mismatch of EB-OCC in post-processing. Specifically, we demonstrate that awareness of the analog timing issues allows the design of a simple compensation extracted directly from the data packet which helps reduce the mismatch, resulting in a channel capacity increase up to 75 kbps for a single pixel receiver. We additionally demonstrate that because of the ability to transmit at higher rates, tracking of the beacon during high rates of scene motion can be accomplished with lower computational cost than in [9] which allows beacon location updates at higher rates; this effectively reduces the penalty for

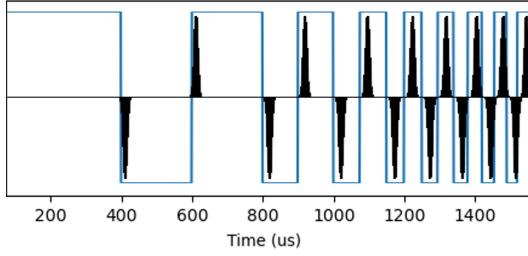


Figure 1. The “binary chirp” experiment. Event-based sensor observes an emitter (LED) displaying a pulse train (blue) with decreasing temporal widths. Histogram of the observed inceptive event (see (6)) is superimposed (black), where the events of negative polarity shown as negative histogram. The timing delay of the events worsens with the decreasing pulse width. (External synchronization trigger was used to ensure there is no clock drift between the emitter and the EBS.)

scene motion from 50% capacity loss to 10% capacity loss at equivalent motion to [9].

The contributions of this work are as follows:

- A method to increase channel capacity of EB-OCC without spatial multiplexing by decoupling the synchronization signal and data packet rates
- A method to further increase channel capacity of EB-OCC, by correcting for undesired characteristics of the event-based sensor’s analog circuit
- A method to compensate for scene motion at lower computational cost facilitated by higher transmission rate signals, allowing decreased channel capacity loss

2. Background

2.1. Event-Based Sensor

An EBS pixel, at location (x, y) , observing intensity $f_{x,y} : \mathbb{R}^+ \rightarrow \mathbb{R}^+$ is designed to asynchronously encode a change in log-intensity exceeding a user-defined *contrast threshold* $\theta \in \mathbb{R}^+$ occurring at time $t \in \mathbb{R}^+$ [2, 3, 5, 6]:

$$|\log(f_{x,y}(t)) - \log(f_{x,y}(t_0))| > \theta \quad (1)$$

for some reference time $t_0 \in \mathbb{R}^+$. The i th recorded event at a pixel $(x, y) \in \mathbb{Z}^2$ is represented as follows:

$$e^i(x, y) = (e_p^i(x, y), e_t^i(x, y)), \quad (2)$$

where

$$e_t^i(x, y) = \min_{\tau \in [e_t^{i-1}(x, y), \infty)} \{ \tau : |\log(f_{x,y}(\tau)) - \log(f_{x,y}(e_t^{i-1}))| > \theta \} \quad (3)$$

is a timestamp at which the event occurs, and

$$e_p^i(x, y) = \text{sgn} \left\{ \log \left(\frac{f_{x,y}(e_t^i(x, y))}{f_{x,y}(e_t^{i-1}(x, y))} \right) \right\} \quad (4)$$

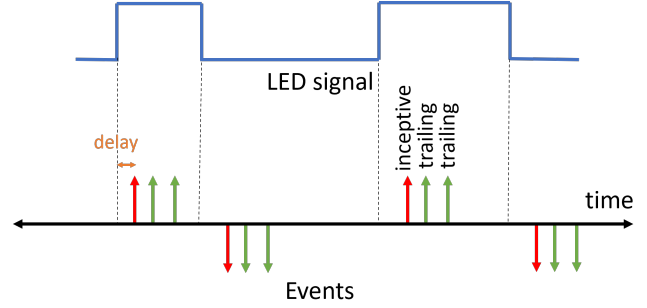


Figure 2. Event-based sensor’s response to binary modulation. The timing of the event polarity change—as indicated by *inceptive events*—detects the presence of binary signal edge, albeit with unknown delay.

is the sign of log-intensity gradient referred to as the *polarity* of the event.

The temporal resolution is effectively 1MHz, making it well suited for high speed communications. A major advantage to the EBS camera is that the true sampling rate of each pixel is spatially independent and temporally signal-dependent, which allows the event streams to reduce data volume by as much as 4 orders of magnitude compared to a frame-based high speed camera by having near-zero data rates on pixels that do not contain the highly temporally dynamic intensity information.

In order to achieve this highly efficient temporal sampling, the magnitude information of the signal is compressed in a lossy fashion which causes the EBS camera to be inefficient at accurately measuring continuous amplitude signals; the transmission scheme we propose in the following section avoids this inefficiency while taking full advantage of the temporal sampling.

3. Signal Analysis of EB-OCC

3.1. Principles of Event-Based On-Off Keying

Consider binary modulation (on or off) of a light source as a physical transmission channel, which is being observed by an EBS acting as a change detector. This offers the highest probability of edge detection, with the goal to take advantage of the high temporal resolution to report level crossing timing. One such encoding scheme is OOK where some sample clock rate f is agreed upon by the transmitter and receiver. The transmitter simply sends a high signal when a digital 1 is sent and a low signal when a digital 0 is sent, which can easily be sent via a blinking LED (the “beacon”) at high rates.

Suppose an EBS pixel (x, y) observes a non-stationary LED-based transmitter at a distance. Let $(x_b(\tau), y_b(\tau))$ denote the trajectory of the beacon’s pixel location at time τ (which we will track in Section 5). Then one can identify

beacon-induced events, EB, as events satisfying the following condition:

$$EB = \left\{ e^i \mid e_t^i(x_b(\tau), y_b(\tau)) = \tau \right\}. \quad (5)$$

For sake of notational simplicity, we let $\hat{e}^i = (\hat{e}_p^i, \hat{e}_t^i) \in EB$ denote time-ordered events in EB.

As illustrated in Figure 2, each 0-to-1 or 1-to-0 modulation change in the emitted signal generates multiple positive or negative events in EBS, respectively. We partition the resultant event stream into *inceptive event* (IE) and *trailing events* (TE), as follows[1]:

$$IE = \left\{ \hat{e}^i \in EB \mid \hat{e}_p^i \neq \hat{e}_p^{i-1} \right\} \quad (6)$$

$$TE = \left\{ \hat{e}^i \in EB \mid \hat{e}_p^i = \hat{e}_p^{i-1} \right\}. \quad (7)$$

Intuitively, the timing of the first polarity change event (inceptive event) corresponds to the signal edge (with delay). The number of trailing events at each edge is roughly proportional to the log-signal edge magnitude; however, trailing events do not provide additional information about the timing of the edge due to serial readout.

The inceptive events of EB, IE, can reconstruct the continuous time OOK signal $s : \mathbb{R} \rightarrow \{0, 1\}$:

$$s(t) = \sum_{\hat{e} \in IE} \hat{e}_p \phi(t - \hat{e}_t), \quad (8)$$

where $\phi(\cdot)$ is a unit step function, and without loss of generality, we assumed that the very first event in the set IE has positive polarity.

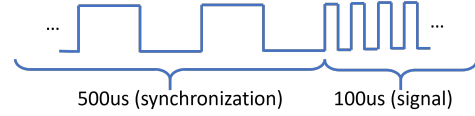
We would like to recover an estimate \hat{b}_k of the transmitted binary signal $b_k : \mathbb{Z} \rightarrow \{0, 1\}$ from the recovered continuous-time OOK signal $s : \mathbb{R} \rightarrow \mathbb{R}$ by temporally sampling $s(t)$ at sampling rate f :

$$\hat{b}_k = s \left(\frac{k}{f} + \Delta_{sync} - \Delta_k \right). \quad (9)$$

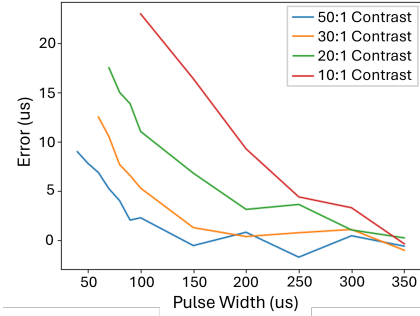
In the ideal case, the global timing delay Δ_{sync} (obtained from a synchronization scheme agreed upon by the transmitter and the receiver) suffices for correcting the timing issues between the received event stream and the reconstruction. Without the additional signal-dependent timing correction Δ_k , however, bit error rate is high due to signal-dependent delay. The remainder of the paper will be dedicated to estimating $(\Delta_{sync}, \Delta_k)$.

3.2. Analysis of Event Timing Delay

The novel insight that we consider in this paper is that the analog circuit architecture of the EBS pixels poses a significant hurdle for high speed signals which cannot be ignored in high transmission rate communication. Specifically, the readout circuitry introduces significant timing errors in events due to noise as well as systematic signal-dependent delay of edge detection timing.



(a) Input LED Signal



(b) Measured Delay

Figure 3. (a) Example LED pattern. The $500\mu s$ pulse train is used to synchronize the camera to the start of the subsequent signal pulses. The $100\mu s$ pulse train represents the “signal” being transmitted. (b) Measuring the relative timing delay of events (the timing “error”) generated by the “signal” as a function of pulse width and pulse magnitude. The delay grows with shorter pulse duration which is exacerbated by smaller contrast.

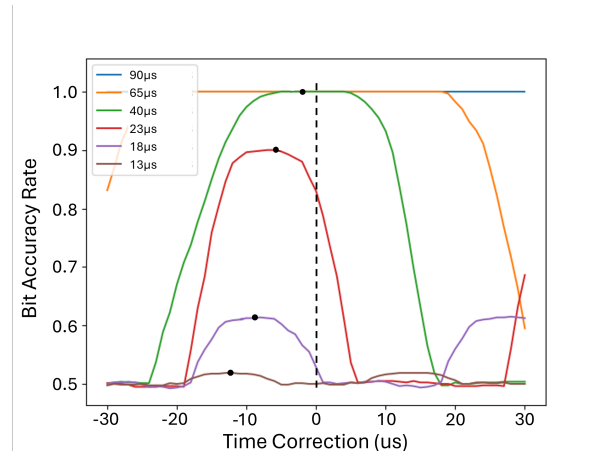


Figure 4. Bit accuracy is dependent on both the probability of detecting a pulse as well as the time at which the declaration is made. For high transmission rate, the time must be corrected (black dots represent ideal corrections, black dash represents correction from slower sync signal only) or else the error will be artificially larger than the physical channel allows. Additionally, a frame sync signal must be sufficiently low transmission rate so that it is detected even for low contrast signals.

To examine this problem more closely, we conducted an experiment to measure the signal-dependent timing delay of EBS sensor empirically by observing periodic con-

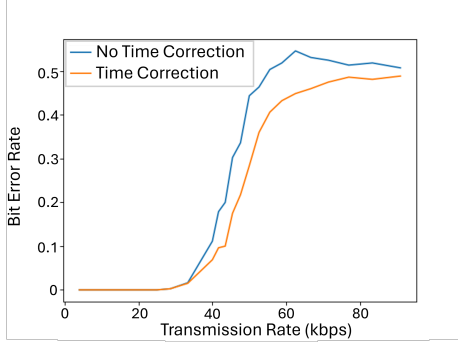


Figure 5. Bit errors using time from frame sync signal (blue) and omniscient delay correction (orange). Without a delay correction, there is an average 10% larger error than the physical transmission channel supports.

stant pulse width LED signals. As shown in Figure 3(a), the LED emits a $500\mu s$ pulse train that we regard as the *frame synchronization signal*, followed by a shorter pulse train ($100\mu s$ in the example) to represent a high transmission rate message.

We report the *relative timing delay* (or “timing error”) of the inceptive events generated by the shorter pulse train, relative to the timing of the inceptive events generated by the $500\mu s$ pulse train. As evidenced by Figure 3(b), the average timing error of the event-based edge detection depends on both the pulse width (inversely proportional to the signal temporal frequency) and the pulse magnitude (contrast) of the LED signal. At $350\mu s$ pulse width, the timing delay relative to $500\mu s$ pulse width is negligible. However, the measured relative timing error grew with the narrowed pulse width and worsened with decreased pulse magnitude due to the analog circuit transfer function.

From this experiment, we observe that the timing of the inceptive events drifts away from the chirp signal’s on-off transitions as the pulse widths of the binary chirp decrease. The cause of this is *not* the clock drift between the emitter and the EBS hardware, as external synchronization signal was used as a time reference. Instead, we attribute this delay to the transfer function (temporal frequency-dependent response to analog signal) of the typical EBS circuit architecture in [5], introducing a signal-dependent timing offset of the recorded inceptive events. Combined with the presence of event timing noise (the timing jitter) and the pixel-to-pixel variation in contrast threshold (the so-called fixed pattern noise), the minimum resolvable pulse widths (which needs to be finer than $1/f$) are severely limited by the timing ambiguities that increase the bit error rate in the transmission.

Next, we quantify the impact of the timing delay and noise (timing jitter) on the OOK sampling in (9). Continuing to use the input LED signal in Figure 3(a), we set the

sampling rate f to the inverse of pulse width (i.e. twice the square signal frequency). We then reconstructed the OOK signal $s : \mathbb{R} \rightarrow \{0, 1\}$ in (8) and sampled according to (9) to yield the binary sequence $b_k : \mathbb{Z} \rightarrow \{0, 1\}$. Without loss of generality, let Δ_{sync} denote the global synchronization timing as measured by the $500\mu s$ pulse train. We compute the resultant bit accuracy rate for a sweep of Δ_k from $-30\mu s$ to $30\mu s$. If the sampling was perfect, then the decoded message would be $\{101010\dots\}$.

Fig. 4 shows the bit accuracy rate of the decoded message as a function of the time correction $\Delta_k \in [-30\mu s, 30\mu s]$ (with a fixed pulse contrast). There are several trends that we observe. First, the bit accuracy of the decoded message does not peak at $\Delta_k = 0\mu s$ —instead, the actual measured accuracy improves when the synchronization timing Δ_k has a negative value. Unfortunately, there is no single value of Δ_k that would be optimal for all pulse widths. The performance boundary is sharp, in fact. For example, the bit accuracy of the $23\mu s$ pulse width pulse train (red curve) drops from 90% at its peak at $\Delta_k = -8\mu s$ to 80% at $\Delta_k = 0\mu s$, which translates to a 50% loss of channel capacity. Second, the bit accuracy deteriorates with decreasing pulse width. This is not unexpected because the probability of edge detection decreases with the pixel read-out circuit’s transfer function that attenuates the edge magnitude.

Figure 5 shows this effect across transmission rates where for rates beyond 30 kbps, fixing $\Delta_k = 0\mu s$ causes an unnecessary 10% increase in bit error rate compared to the minimum obtainable error rate. This is an important observation, as there is a large loss of channel capacity inherited by potentially correctable sampling time, and not by the transmission channel itself. Real-world OOK signals encoded with actual binary messages have irregular edges (i.e. not periodic like the pattern illustrated in Figure 3(a)), thus the signal-dependent delay is not constant throughout the OOK signal (conceptually similar to a *mixture of pulse width*), but the most difficult bits to recover will always be the maximum switching frequency because the transfer function attenuates high frequencies the most. As already evidenced in Fig. 4, the penalty stemming from inaccurate time correction is smaller for wider pulses. Therefore, we seek to correct for the maximum switching frequency as described in the next section.

4. Proposed Synchronization Strategy

Recall (9). To achieve a microsecond-order precision in signal synchronization, we propose a phase-locked loop-inspired method that utilizes two stages of timing correction. The first stage estimates the global temporal offset Δ_{sync} using a frame synchronization signal. The second stage estimates the signal-dependent timing correction Δ_k . Once $(\Delta_{sync}, \Delta_k)$ are estimated, the binary code is esti-

mated via sampling in (9).

4.1. Frame Synchronization

The first stage of time correction uses a simple frame synchronization signal $s_f : \mathbb{R} \rightarrow \mathbb{R}$ with a fixed-width pulse train to identify the beginning of a data frame within $\pm 30\mu s$:

$$s_f(t) = \sum_{k=1}^{2K} (-1)^k \phi(t - kw), \quad (10)$$

where w is the pulse width, and K is the number of pulses. This signal is appended to the beginning portion of a data packet $s : \mathbb{R} \rightarrow \mathbb{R}$ to form the frame. All channel capacities reported in this work account for the length of this frame synchronization signal since it carries a transmission overhead. Pulse width w should be chosen to be slower than the transmission rate (i.e. $w > 1/f$) in order to reduce the likelihood that a frame is completely missed. We contrast this to methods in [10] and [9] that send the frame synchronization signal at the transmission rate, causing significant numbers of missed frames at high transmission rates.

To search for frame synchronization signal in event stream, we considered two cost functions:

$$r(i) = \sum_{k=1}^{2K} ((\hat{e}_t^{i+k} - \hat{e}_t^i) - kw)^2 \quad (11)$$

$$\tilde{r}(i) = \sum_{k=1}^{2K} ((\hat{e}_t^{i+k} - \hat{e}_t^{i+k-1}) - w)^2, \quad (12)$$

where $\hat{e}^i \in \text{IE}$ represent inceptive events in (6). Intuitively, $r(i)$ and $\tilde{r}(i)$ are measures of deviation from periodicity of event timing by w . Thus the global synchronization is the minimizer of $r(i)$ or $\tilde{r}(i)$:

$$\hat{\Delta}_{sync} = \hat{e}_t^{\hat{i}}, \quad \hat{i} = \arg \min_i r(i), \quad (13)$$

where we impose an additional constraint that $r(\hat{i})$ must be below a user-defined threshold value before declaring that $\hat{\Delta}_{sync}$ is valid.

We may assess the accuracy of $\hat{\Delta}_{sync}$ based on the external trigger to the system. In practice, the global delay $\hat{\Delta}_{sync}$ estimated by (11) and (12) were within $5\mu s$ and $10\mu s$ of the frame start time, respectively. Note however that cost function $r(i)$ in (11) is vulnerable to missed events or noise events recorded during the synchronization time, while cost function $\tilde{r}(i)$ in (12) can tolerate some amount of misses and noise.

4.2. Signal Delay Compensation

The second stage of time correction utilizes the transmitted message data itself to locally refine the timing delay estimates $\hat{\Delta}_k \in [\Delta_k - 3\mu s, \Delta_k + 3\mu s]$. There is no additional

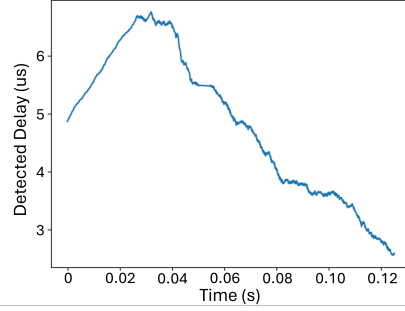


Figure 6. Example of delay detection through time. Over 0.12 seconds, the delay fluctuates due to changes in contrast as the scene is moving at 55 deg/s.

transmission overhead to this technique, thanks to the fact that no synchronization signal is needed, and therefore the correction Δ_k can be continuously estimated and applied for the entire duration of the data packet transmission.

Based on the model in (9), each event $\hat{e} \in \text{IE}$ is assumed to be generated from a pulse transition with an unknown timing delay

$$\hat{e}_t = \frac{k}{f} + \Delta_{sync} - \Delta_k \quad (14)$$

for some value $k \in \mathbb{Z}$, and Δ_k is the unknown delay on the signal at the k th clock cycle. To estimate Δ_k , we take a nearest neighbor approach to minimize the error between $\frac{k}{f} + \Delta_{sync}$ and \hat{e}_t , as follows:

$$\hat{k} = \text{round} \left((\hat{e}_t - \hat{\Delta}_{sync}) f \right) \quad (15)$$

Then the delay Δ_k is *initially* estimated as the residual:

$$\tilde{\Delta}_{\hat{k}} = \left(\frac{\hat{k}}{f} - \hat{\Delta}_{sync} \right) - \hat{e}_t. \quad (16)$$

Notice that no valid delay estimate for $\tilde{\Delta}_{\hat{k}}$ exists at k when an event is not observed around the time k/f .

Finally, we account for noise in the delay estimates. We filter this initial delay estimate to arrive at final delay estimate:

$$\hat{\Delta}_k = \begin{cases} \alpha \tilde{\Delta}_k + (1 - \alpha) \hat{\Delta}_{k-1} & \tilde{\Delta}_k \text{ is valid} \\ \hat{\Delta}_{k-1} & \text{else,} \end{cases} \quad (17)$$

where α is a parameter to control the degree of smoothing. An example estimate of $\hat{\Delta}_k$ is shown in Figure 6.

5. Motion Compensation

5.1. Algorithm

In OCC, it is necessary to compensate for motion of the transmitter/receiver to maintain high accuracy. Despite the

very high computational cost, the accuracy of EB-OCC motion compensation technique in [9] employing optical flow was limited. We propose a much more simplistic but effective method for tracking the transmitter when operating at high transmission rate; this method works due to the improvement in transmission rates over [9].

We begin with the assumption that the transmitted signal always occupies a minimum of kHz switching frequency; in our study transmission rates can operate from 1kHz to 100kHz with ideal transmission rates being in the 25kHz range. Because of this, our proposed beacon detection algorithm can rely on event counting alone. Let τ be time window. Then the event accumulation is

$$A(x, y, t) = \#\left\{e^i(x, y) \mid t - \frac{\tau}{2} \leq e_t^i(x, y) < t + \frac{\tau}{2}, e_p^i(x, y) \neq e_p^{i-1}(x, y)\right\}, \quad (18)$$

where $\#\{\cdot\}$ is the cardinality of the set. See Figure 7 (a). The transmitter is identified by thresholding $A(x, y, t)$ since the event rate of the transmitter is expected to be significantly higher than the temporal dynamics of the natural scene. We take the centroid of connected pixels above the threshold to find the beacon's pixel location $(x_b(t), y_b(t))$ in (5).

Note that EBS typically have some “hot pixels” that continuously generate events (yielding high event accumulation in (18)). Fortunately, they are easy to discard because the locations of the hot pixels can be known *a priori* (put lens cap on the camera, threshold by event rate) and can simply be masked out of $A(x, y, t)$. Alternatively, because the transmitter is expected to occupy multiple pixels in a well sampled system (i.e. have connected neighbors), one can perform binary morphological operations to remove pixels that do not have connected neighbors. For instance, a 3×3 erosion followed by 3×3 dilation removes isolated pixels that passed the initial thresholding step (hot pixels or small bright objects).

Lastly, this simplistic motion compensation technique relies on the high transmission rate to separate the beacon from the background clutter. Prior art in EBS-OCC operates at a maximum of 4kbps transmission [9, 10] which is arguably too slow to yield meaningful clutter suppression by thresholding $A(x, y, t)$ in (18).

6. Results

6.1. Experimental Setup

We utilize the RP2040 to store and transfer sufficiently large amounts of data. We buffer the digital output from the GPIO to drive multiple LEDs using National Instruments USB-6353 DAQ. The LED used was a 626nm diode with an integrated 15 deg beam focusing optic which produces up to

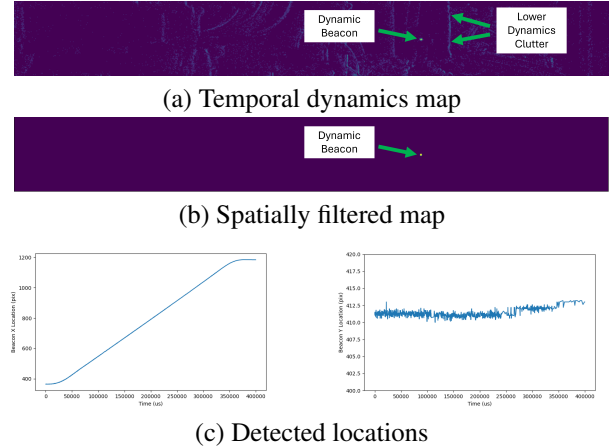


Figure 7. Example of beacon extraction with 60 deg/s motion using $250\mu s$ time windows. Although images are displayed for visualization, in practice this is a sparse calculation directly on event data. After all locations are detected in (c), if there is more than one beacon detected, the detections can be correlated together into tracks and used to assemble beacon polarity from multiple pixels over time.

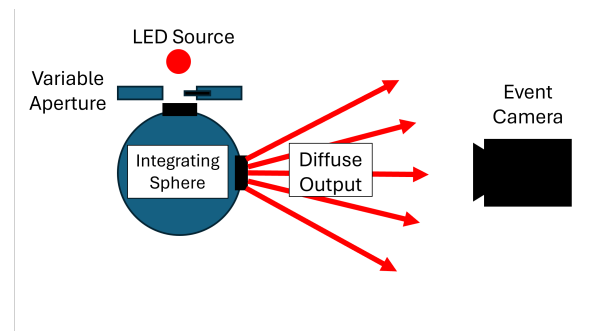


Figure 8. Depiction of static transmitter experimental setup.

21cd maximum output, which has the headroom for future long distance outdoor experiments.

Figure 8 illustrates an experimental setup for the static transmitter. The light from 8 LEDs are injected into a 3 inch Spectralon coated integrating sphere with a variable aperture at the injection port to control the contrast of the output light. Contrast ratios as large as 50:1 with a baseline of ambient room lighting are possible. We tested from 1m away. However, since the light source is large and diffuse, the results obtained in our experiment are expected to hold for longer distance until the source port becomes small relative to the projected area of a pixel ($\approx 50m$ away).

The configuration for the dynamic motion experiment is shown in Figure 9. A single LED is passed through a 1mm pinhole to ensure that the beacon is subpixel at 4m distance. The LED generates maximum output contrast of $\approx 40:1$. An Aerotech direct-drive gimbal with azimuth and elevation

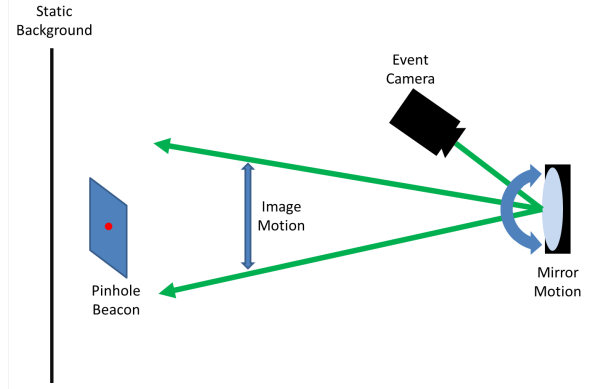


Figure 9. Depiction of dynamic motion experimental setup.

control is used to induce motion of the entire static background, simulating camera movement. A constant velocity of 0 to 60 deg/sec is programmed in the azimuth direction with a fixed elevation, which induces a constant pixel velocity in the camera's horizontal direction. The mirror's large clear aperture did not affect the image quality or introduce undesired vignetting. After considering the folded path with the mirror in place, the test distance was set to 4m.

The experiments were conducted using a Prophesee EVK4 (Sony IMX636ES, 1280×720 pixels) paired with a 12mm lens, yielding a 30 degree field-of-view. The pixels were biased to have the largest bandwidth allowable and the smallest threshold for the static transmitter experiments. For the dynamic transmitter motion experiments, the contrast threshold was set to the default to reduce the total number of events being generated from the background clutter.

6.2. Evaluation Metrics

We report bit accuracy rate (BAR), message accuracy rate (MAR), and channel capacity as defined in the following section. Let \hat{b}_k be the k th recovered bit and b_k be the k th transmitted bit. BAR is defined as

$$B = \frac{1}{N} \sum_{k=0}^{N-1} \delta[b_k - \hat{b}_k], \quad (19)$$

where $\delta[\cdot]$ is the Kronecker delta. BAR is an estimate of the probability that a recovered bit is equal to its corresponding transmitted bit. Let $m_k = \sum_{\ell=0}^7 2^\ell b_{8k+\ell}$ and $\hat{m}_k = \sum_{\ell=0}^7 2^\ell \hat{b}_{8k+\ell}$ be the k th transmitted and recovered 8-bit symbol. MAR is defined similarly to BAR as

$$M = \frac{1}{N} \sum_{k=0}^{N-1} \delta[m_k - \hat{m}_k]. \quad (20)$$

Channel capacity C is calculated from entropy H , under the assumption of uncorrelated errors, as follows:

$$H = -(1 - B) \log_2(1 - B) - B \log_2(B) \quad (21)$$

$$C = (1 - H) \left(\frac{N}{f} + 2Kw \right)^{-1}, \quad (22)$$

where N is the number of bits in a data packet, and Kw is the frame synchronization signal duration (modified for signal different than constant width pulse train).

As BAR approaches 1, channel capacity approaches its theoretical maximum at $\left(\frac{N}{f} + Kw \right)^{-1}$. Conversely, as BAR approaches 0.5, channel capacity converges to 0. Information theory proves that an error correction scheme exists such that the channel capacity can be met with sufficiently small error rate. These correction schemes will be addressed in our future work.

6.3. Experimental Evaluation

For each test conducted, a random sequence of 8-bit words was transmitted with 1000-6000 bits in each data frame. This was repeated 50 times for each test point with errors in the sequence being averaged to produce bit/message accuracy and channel capacity.

Figure 10 and Table 1 present the results of static testing our OOK method outlined in Section 3, along with comparison to limited results found in [10] and [9]. An additional curve for max contrast is given for direct viewing of the LED without the integrating sphere, which removes the calibration diode used to measure contrast. It is clear from the results that the method proposed in this work allows for significantly larger data transmission rates even at relatively low contrast. Based on what was documented[9, 10], we estimate that prior works had between 20:1 and 40:1 contrast.

Figure 11 shows the impact of beacon motion after the post-processing compensation detailed in Section 5.1. Time window of $\tau = 250\mu s$ was used for transmitter detection. The experiment was fixed as a 25 kbps transmission rate with 5 repetitions of $73\mu s$ wide on-off pulses as the frame synchronization sequence. Each data frame contains 3128 bits which takes approximately 125ms to transmit. Two stage global timing ($\hat{\Delta}_{sync}$) and signal-dependent delay correction ($\hat{\Delta}_k$) is superior to the one stage correction ($\hat{\Delta}_{sync}$ only) for all motion rates. Both synchronization methods improved the result in [9] from less than 1350 bps channel capacity to at least 13000 bps.

7. Conclusion

We proposed and demonstrated a method for increasing the channel capacity of On-Off Keying (OOK) Event-Based Optical Camera Communication (EB-OCC) by a factor of 25× over the prior art. We additionally demonstrated that

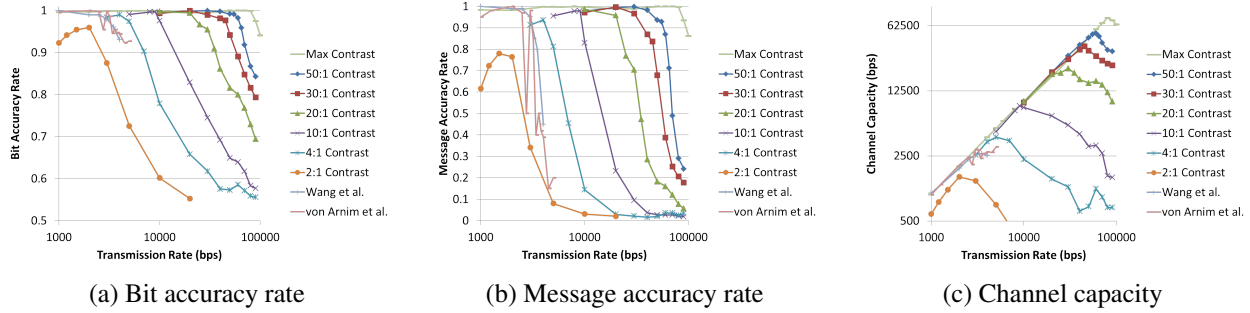


Figure 10. Results of static laboratory testing for bit transmission rates from 1 kbps to 100 kbps. The method proposed in this work exceeds the performance of [10] and [9] in all metrics for contrasts above 4:1.

Contrast	Bit Rate @ BAR=99%	Bit Rate @ MAR=90%	Maximum Capacity (bps)
Max Contrast	84112	93651	75777
50:1	55504	57411	51706
30:1	29603	33409	37611
20:1	20823	21523	21774
10:1	9336	9530	8624
4:1	4005	4293	3979
2:1	*	*	1488
Wang et al. [10]	≈ 2500	≈ 3200	≈ 2650
von Arnim et al. [9]	≈ 3200†	≈ 3200	≈ 2900†

Table 1. Selection of results of static laboratory testing for comparison to values found in prior works. The method proposed in this work exceeds performance in [10] and [9] for all values when contrast is larger than 4:1.

* Camera bias conditions used to increase performance at high contrast cause significant error rates at low contrast.
 † Upper bound of BAR estimated from reported MAR with only one bit error per 11-bit message.

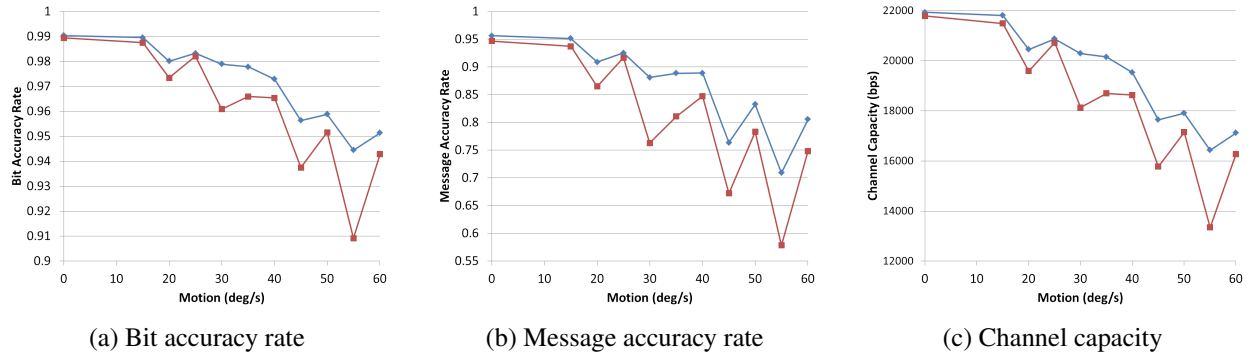


Figure 11. Motion compensation results for a 25 kbps transmission with one stage timing correction (red) and two stage timing correction (blue) under various rates of motion. Two stage timing correction averages 1% better bit accuracy, 8% better message accuracy, and 7% better channel capacity than one stage timing correction.

this higher transmission rate simplifies beacon identification and motion compensation methods, enabling higher rates of compensation which reduces capacity loss. We performed experiments with stationary and moving transmitters using real-world emitter and event-based sensor hardware to confirm substantial improvements.

References

[1] R Baldwin, Mohammed Almatrafi, Jason R Kaufman, Vijayan Asari, and Keigo Hirakawa. Inceptive event time-surfaces for object classification using neuromorphic cameras. In *International conference on image analysis and recognition*, pages 395–403. Springer,

2019. [3](#)

- [2] Tobi Delbrück, Bernabe Linares-Barranco, Eugenio Culurciello, and Christoph Posch. Activity-driven, event-based vision sensors. In *Proceedings of 2010 IEEE International Symposium on Circuits and Systems*, pages 2426–2429. IEEE, 2010. [2](#)
- [3] Thomas Finateu, Atsumi Niwa, Daniel Matolin, Koya Tsuchimoto, Andrea Mascheroni, Etienne Reynaud, Pooria Mostafalu, Frederick Brady, Ludovic Chotard, Florian LeGoff, et al. 5.10 a 1280× 720 back-illuminated stacked temporal contrast event-based vision sensor with 4.86 μm pixels, 1.066 gepps readout, programmable event-rate controller and compressive data-formatting pipeline. In *2020 IEEE International Solid-State Circuits Conference-(ISSCC)*, pages 112–114. IEEE, 2020. [2](#)
- [4] Mohammad Ali Khalighi and Murat Uysal. Survey on free space optical communication: A communication theory perspective. *IEEE communications surveys & tutorials*, 16(4):2231–2258, 2014. [1](#)
- [5] Patrick Lichtsteiner, Christoph Posch, and Tobi Delbrück. A 128×128 120 db 15 μs latency asynchronous temporal contrast vision sensor. *IEEE journal of solid-state circuits*, 43(2):566–576, 2008. [2](#), [4](#)
- [6] Christoph Posch. Bio-inspired vision. *Journal of Instrumentation*, 7(01):C01054, 2012. [2](#)
- [7] Nirzhar Saha, Md Shareef Ifthekhar, Nam Tuan Le, and Yeong Min Jang. Survey on optical camera communications: challenges and opportunities. *Iet Optoelectronics*, 9(5):172–183, 2015. [1](#)
- [8] Hang Su, Ling Gao, Tao Liu, and Laurent Kneip. Motion-aware optical camera communication with event cameras. *IEEE Robotics and Automation Letters*, 2024. [1](#)
- [9] Axel Von Arnim, Jules Lecomte, Naima Elosegui Borras, Stanisław Woźniak, and Angeliki Pantazi. Dynamic event-based optical identification and communication. *Frontiers in Neurobotics*, 18:1290965, 2024. [1](#), [2](#), [5](#), [6](#), [7](#), [8](#)
- [10] Ziwei Wang, Yonhon Ng, Jack Henderson, and Robert Mahony. Smart visual beacons with asynchronous optical communications using event cameras. In *2022 IEEE/RSJ International Conference on Intelligent Robots and Systems (IROS)*, pages 3793–3799. IEEE, 2022. [1](#), [5](#), [6](#), [7](#), [8](#)